ORIGINAL ARTICLE

Chemical and mineralogical characterization of weathering products in mine wastes, soil, and sediment from the abandoned Pb/Zn mine in Skikda, Algeria

Malika Khelfaoui[1,2] · M. S. Medjram[1,2] · Abdenour Kabir[3] · Daoiya Zouied[2] · Karima Mehri[2] · Olfa Chikha[4] · Malika Ayadi Trabelsi[4]

Abstract

The Sidi Kamber Zn/Pb mine located 60 km from Skikda is one of the abandoned mining areas of northeastern Algeria for more than 40 years. Currently, this mining area is considered as a real environmental problem. The purpose of this work is to identify and characterize different sources of polymetallic pollution and their impact on the Guénitra dam sediments quality by analyzing the metal content of the weathering products in mine wastes (tailings and waste rock), soil affected by acid mine drainage and Guenitra dam sediments. Moreover, this study aims to determine the mineralogical composition of new compounds occurring in the fine-grained sediments (less than 250 μm) of the mining area. The chemical analysis and the concentration of Fe, Cd, Zn, Cr, Pb, Cu, Mn, Ni, and Hg metals of the studied samples were performed using atomic absorption spectroscopy analysis, inductively coupled plasma optical emission spectrometer, and X-fluorescence ray analysis. The mineralogical composition of all samples was characterized by several techniques such as Fourier transform infrared spectroscopy, X-ray diffraction, scanning electron microscopy, and energy-dispersive spectroscopy. The obtained data were analyzed using multivariate statistical analysis, correlation matrix, hierarchical cluster analysis (HCA), and principal component analysis (PCA). The results showed very high content of Pb, Zn, Cd, Cr, and Hg toxic metals in all samples and suggest taking corrective measures should be taken to reduce the spread of these hazardous elements into the environment. A rehabilitation of the abandoned Sidi Kamber mine should be recommended, as well. The obtained results of HCA and PCA suggest two principal origins of metals pollution: Cu, Mn, Hg, and Pb are derived from anthropogenic sources of mine wastes from the tailings piles, while, Ni, Zn, Cr, and even Fe are derived from lithogenic and anthropogenic sources. Mineralogical characterization results of weathering products in mine wastes, soil, and sediment highlighted the presence of the following minerals: quartz, muscovite, kaolinite, goethite, hematite, lepidocrocite, ferrohexahydrite, and jarosite.

Keywords Metals · Soil · Sediment · Mine wastes · Mineralogical characterization

✉ Malika Khelfaoui
m.khelfaoui@univ-skikda.dz

1 Laboratory LGCES, Faculty of Technology, 20 Août 1955 University, El-Hadaeik Road, P.O. Box 26, 21000 Skikda, Algeria

2 Department of Petrochemistry and Process Engineering, Faculty of Technology, 20 Août 1955 University, P.O. Box 26, 21000 Skikda, Algeria

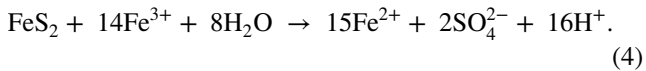3 Laboratory LRPCSI, Faculty of Sciences, 20 Août 1955 University, El-Hadaeik Road, P.O. Box 26, 21000 Skikda, Algeria
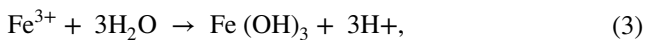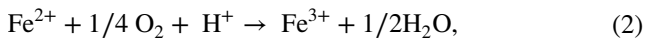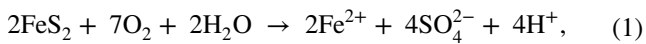
4 Laboratory (LACReSNE), Faculty of Sciences of Bizerte, 7021 Zarzouna, Tunisia

Introduction

The mining industry and the extraction of metal ores constitute a significant source of environmental contamination by heavy metals (Dudka and Adriano 1997; Singh et al. 2015; Navarro et al. 2008); mining activities affecting sulfide minerals usually result in the excavation of a huge amount of anoxic subsoil rock which can be exposed to the surface oxic environment (Hochella et al. 2005; Silva et al. 2013). The exposition of waste rock to water, oxygen, and bacteria may cause metal leaching and the formation of acid mine drainage (AMD).

Metal sulfide oxidation is a complex process that includes several redox reactions (1–4), which are controlled by the

geology, microbiology, and climate of each area (Acero et al. 2006):

$$2FeS_2 + 7O_2 + 2H_2O \rightarrow 2Fe^{2+} + 4SO_4^{2-} + 4H^+, \quad (1)$$

$$Fe^{2+} + 1/4\,O_2 + H^+ \rightarrow Fe^{3+} + 1/2H_2O, \quad (2)$$

$$Fe^{3+} + 3H_2O \rightarrow Fe\,(OH)_3 + 3H+, \quad (3)$$

$$FeS_2 + 14Fe^{3+} + 8H_2O \rightarrow 15Fe^{2+} + 2SO_4^{2-} + 16H^+. \quad (4)$$

These reactions occur in parallel and last as long as there is access to air and water. Rios et al. explained in detail this phenomenon of pyrite decomposition (Rios et al. 2008; Iakovleva et al. 2015).

The closure of any mine requires, as a last step, necessary and special measures to reduce AMD generating processes that are the main sources of pollution, with levels being even more significant than in their period of activity. In abandoned mines, AMD can be produced by oxidation of sulfides occurring in underground and open-air excavations, as well as in tailings and waste rock dumps (Favas et al. 2016). Tailings are solid wastes that are produced by the mining procedure; they contain dangerous and toxic elements that tend to seep into the surrounding environment by water runoff (Zanuzzi et al. 2009; Rowe and Hosney 2013). Unfortunately, these tailings are most often left without treatment or management in the mining areas. Their unseemly management may cause heavy metal migration in the surrounding area, causing soil and water contamination, as well as landscape degradation and a decrease in biological diversity (Rashed 2010). Besides, groundwater rich in oxygen circulating in the abandoned mine may trigger and/or accelerate the oxidation process of metal sulfides, thus generating AMD and causing extensive precipitation of sulphates and Fe oxides and/or oxyhydroxides; it should be noted that the precipitates of hyrdoxysulfates and Fe oxyhydroxides are abundant minerals in AMD. According to several studies, these latter retain SO_4^{2-} at low pH (Rose and Elliott 2000; Kim et al. 2002; Choo and Lee 2002), and can also be influenced by the presence of metal ions and other complexing ligands. Jarosite can form at pH < 3 and high concentrations of SO_4^{2-}. As pH increases, ferrihydrite, schwertmannite, and goethite are known to precipitate. Lepidocrocite was precipitated at pH 7; while at a pH below 5.5, a mixture of goethite, schwertmannite, ferrihydrite, and lepidocrocite have formed (Bigham and Murad 1997; Bigham et al. 1996; Jonsson et al. 2006).

Additionally, runoff from tailings piles and waste rocks can carry large amounts of metal as precipitation infiltrates the piles and promotes geochemical weathering of primary minerals containing metal (Tonkin et al. 2002; Laurel et al. 2014). These phenomena are noticed in Sidi Kamber (Pb/Zn) mine, located in Skikda (northeast Algeria) at about 2 km upstream of Guenitra dam. Although this mine has been abandoned, its harmful effects on water and soils have remained till our day. Only two studies have been carried out in this region. The first study (Bouhkalfa 2007) showed a significant level of waters and sediments' pollution of El-souk river by Fe, Mn, Zn, Pb, and Cd metals, whereas the second one (Boukhalfa and chaguer 2012) dealt with the sediments characterization of this river. However, no previous studies have been tackled on the different sources of pollution by Fe, Cd, Zn, Cr, Pb, Cu, Mn, Ni, and Hg metals and their impact on the surrounding soil and Guénitra dam sediments.

The purpose of this study is threefold: (1) identifying the different sources of environmental pollution by heavy metals in the area, (2) determining the concentration of metals in weathering products in mine wastes (tailings and waste rocks), soil affected by AMD and Guenitra dam sediments to assess their environmental impacts, and (3) characterizing the mineralogical composition of the very fine compounds less than 250 μm occurring in mine wastes, soil affected by AMD, and sediments of Guenitra dam.

Materials and methods

Study area and sampling procedures

The Sidi Kamber abandoned Zn/Pb mine is located northeast of Algeria, 60 km from Skikda and 70 km from Constantine. The climate of the Mediterranean region of Sidi Kamber is a semi-arid with dry and hot summers and wet winters, with a mean annual rainfall of about 600 mm and a sparse vegetation cover (Bouhkalfa 2007). The relief contains mountains with altitudes varying between 200 and 500 m. The slopes vary between 2 and 25% (Gherib et al. 2017). The beginning of mining activities goes back to the Roman time, but industrial exploitation operations began in 1890, with a limited production and quite frequent interruptions. Starting from 1913, the mine began to have a regular activity. In 1938, the Sidi Kamber mine produced 678 tons of galena and 146 tons of blende, occupying an area of about 2271 ha. In 1976, the exploitation of Pb and Zn deposits was stopped, but the open-cast mining production of barite was continued until 1984, when the Sidi Kamber mine was closed (Oumedjbeur 1986). The geological nature of the area, composed of sandstone and clay, gives low permeability to the soil. There are several metalliferous grounds in the region, including the Sidi Kamber and the Djebel dar El-Debbar mines.

The deposits of the Sidi Kamber mine consist of a series of metalliferous veins with sulfide mineralization. The composition of the ore minerals is as follows:

- Galena PbS (Pb 86.6%, S13.4%, Ag 1%, Cr, Zn, Se, Bi, Sb, Mo);
- Sphalerite ZnS (Zn 67.1%, S 9%, Fe up to 20%);
- Barite $BaSO_4$ + Cd, In, Ca, Mn, Sn, Hg. Rarely marcasite, pyrite, chalcopyrite, pyrrhotite, and, sometimes, small crystals of quartz and calcite (Beddai 1976).

El-souk river, one of the tributaries of the Guenitra dam, is still affected by runoff from mining waste (waste rocks and tailings) (Oumedjbeur 1986).

The Guénitra dam is located in the Skikda province—Algeria, about 60 km south from the province chief town, with a surface area of 900 ha, a gross capacity of 125 million m^3, and a useful capacity of 115.5 million m^3. This dam has a dual purpose: it supplies drinking water supply to the Skikda city (37,000 m^3 and 199,921 people), its surrounding urban areas, and industrial area (16,000 m^3). Also, it is intended to ensure the irrigation of Emdjez–Edechich

perimeters and the Saf–Saf valley, with an area of 5650 ha (Medjram and malika 2014).

ST, SH, and SW Samples were collected from the Sidi Kamber mine (Fig. 1), close to each source of pollution, and sediment samples SD from the Guenitra dam. According to the extensive research and inspection of the mine site, metal pollution of soils, waters, and sediments in the Sidi Kamber abandoned mine region was noticed to be induced by the three following sources of pollution: tailings piles, waste rock rich in iron oxide and oxyhydroxide, and AMD resulting from leachate of metals and sulphates by groundwater flowing through the former drilling site of the ore during the mining period.

A total of 24 samples have been studied, including 12 samples of weathering products from mine wastes (6 in tailings ST and 6 in waste rocks SW), 6 samples in SH representative of soil affected by AMD, and 6 samples in SD representative of Guenitra dam sediments. The different samples were collected during the spring period of 2016 from four different sites: ST, SH, SW, and SD, in six locations close to each site. The spring period has been chosen to take samples, because it experiences different weather

Fig. 1 Map with the location of the study area showing sampling points SW, SH, ST, and SD

conditions, rainy and dry. A sampling of each site is carried out approximately to the following four positions:

- ST (36°43′04.19″ N, 6°35′15.83″ E) samples of weathering products in tailings piles.
- SH (36°43′00.44″ N, 6°35′20.68″ E) samples of soil affected by AMD near a groundwater seepage.
- SW (36°42′57.56″ N, 6°35′31.53″ E) samples of weathering products in waste rocks.
- SD (36°42′41.01″ N, 6°36′55.40″ E) samples of sediment from the Guénitra dam (Fig. 1).

The depth varying from 0 to 5 cm was determined using a grab sampler. After that, the samples were put in clean plastic bags and then kept at 4 °C for the analysis. 500 g samples of each type of material, namely, weathering products in tailings and waste rocks, soil affected by AMD, and Guenitra dam sediment, were collected at each site to realize several experiments such as mineralogical and chemical compositions. All samples were dried at room temperature, and stones, biological materials, and other impurities were removed. After drying, the samples were ground with agate mortar, so as to pass through a 250 μm nylon sieve to determine metals' concentrations and the mineralogical characterization.

To control the accuracy of metals concentrations, the analytical results were estimated by replicating analysis; each value is expressed as the mean of three replicates. All laboratory equipment used for the experiments are from Pyrex, washed with 0.1 N of HNO_3, then rinsed twice with bi-distilled water, and placed in a stove until dry. Analytical blanks of heavy metal were run similarly as the samples, in the same conditions using the same quantities of reagents. All metal concentrations were determined using standard solutions. The concentrations were expressed in mg/kg dry matter. The precision of measurement error was estimated at $\pm 5\%$ for all results of the analyzed metals.

Chemical analysis procedures

To evaluate the level of environmental pollution caused by metals and semi-quantitative composition of oxides, soil affected by AMD, Guenitra dam sediments SD, and mine wastes (tailings ST and waste rock SW) left in place for more than 40 years were studied. All samples ST, SH, SW, and SD were analyzed for concentration of Pb, Zn, Fe, Ni, Mn, and Cr, using Flame Atomic Absorption Spectrometry (FAAS), equipped with deuterium background correction (Thermo-scientific 3000), at a laboratory owned by GL1K (Liquefied Natural Gas facility, Algeria). On the other hand, the concentrations of metals like Hg, Cd, and Cu, expected to be considerably low, were determined using inductively coupled plasma optical emission spectroscopy (ICP/OES)

Perkin Elmer precisely optima 21000 DV, equipped with a tubes autosampler. Hg was determined by (ICP/OES) hydrides system in Greenlab laboratory, Tunisia. Samples pH was measured using a 2, 5:1 ratio of water to mine wastes, soil, or sediment. Prior to chemical analysis, samples were digested using pseudo-total aqua regia digestion. This was done in closed vessel according to the French standards (NF EN 13346 2000) with slight modifications. This method involved taking 0.25 g of accurately weighed sample in Teflon bombs, to which 6 ml of HCl and 2 ml of HNO_3 were added. Medium pressure vessels were then capped and subjected to a temperature of 110 °C for 2 h. Samples were filtered, quantitatively transferred, and made up to 25 ml in a volumetric flask with ultrapure water. Metals were analyzed using direct calibration under the same conditions as the samples.

The X-ray fluorescence (XRF) was used for semi-quantitative analyses. For this purpose, the samples were treated by the borax fusion method (Tertian and Claisse 1982), which involves fusion at 1050 °C in a platinum nasal crucible of the sample. The latter is mixed with a very small amount of sodium iodide and an excess of di-lithium tetraborate and casting into a solid bead in the oven (XF FUSE 6 SOCACHIM). The samples were analyzed by XRF spectrometry using a thermo-scientific ARL PERFORM'X XRF sequential spectrometer. The results were expressed as weight percent for the major element oxides in each sample. The loss on ignition at 1050 °C for each sample was also determined as part of the analysis process. The XRF analysis was carried out at the laboratory of the Sider El-Hadjar Complex in Annaba, Algeria.

Statistical analysis

To develop the purpose of this study, IBM SPSS Statistics software version 19 was used to apply statistical approaches to the data for 24 samples. Pearson correlation matrix (CM) was used to identify the relationship of the elements, with the concentrations of metals in the columns (09) and the set of samples (24). Hierarchical cluster analysis (HCA) and principal component analysis (PCA) were also used to identify the possible sources of metals. Factor analysis (FA) was performed to minimize the number of variables with a high load on each component, thus facilitating the interpretation of the PCA results.

Mineralogical analysis procedures

Various methods were used to identify and characterize the mineralogical composition of weathering products in mine wastes (tailings and waste rocks), soil polluted by AMD, and Guenitra dam sediments' samples. We have chosen only one sample for each site. The analysis using Fourier

transform infrared spectroscopy (FTIR), X-ray diffraction (XRD), scanning electron microscopy (SEM), and energy-dispersive spectroscopy (EDX) was carried out on different random surfaces.

The minerals in the samples were identified by X-ray powder diffraction (XRD) technique. The analysis was carried out by X-ray diffractometer (Inel Equinox 3000, LRPCSI Laboratory, Skikda), using Cu-Kα radiation and operating in step scan mode between 1° and 100° (2θ), with 0.05° (2θ) steps, and a counting time of 1 min per step was used. The identification and quantification of mineral phases was performed using Symphonix software and ICDD Database (2017).

The binding groups in the selected samples were identified using FTIR spectroscopy (Thermo Scientific Nicolet iS5 FTIR Spectrometer, LRPCSI Laboratory-Skikda). FTIR spectra were analyzed in the wave numbers range between 4000 and 400 cm^{-1} and were processed using OMNIC software in absorbance mode.

The particle morphology of the studied samples was performed by emission scanning electron microscope (SEM, Model: JEOL -JSM-6360LV, CDTA Laboratory, Algeria), and EDX Bruker Quantax 200 energy-dispersive X-ray spectrometer at the CRAPC Laboratory, Algeria.

Results and discussion

Chemical analysis

Variations of Fe, Cd, Zn, Cr, Pb, Cu, Mn, Ni, and Hg metal contents in ST, SH, SW, and SD samples based on statistical analyses are reported in (Fig. 2). The statistical parameters of all samples and the comparison by the two thresholds of pollution levels by metals, fixed by the Italian law are presented in (Table 1); these Italian standards have been used given the lack of Algerian standards. The comparison of iron and manganese by Italian law has not been taken into account. According to (Fig. 2), the concentration values of the same metal in the same site have been noticed to be different; this is due to two reasons, namely, the effect of climate and rainfall in the year and the small spatial variation in sampling, which has a deductive effect despite the close distances between the samples.

Comparing the box plots (Fig. 2) of each element with other metals, Fe, Mn, Zn, and Pb in the region were found to have the highest concentrations, followed by Cd and Ni that had moderate concentrations, whereas Cr, Hg, and Cu had minimal concentrations.

According to Table 1, the mean Pb values of samples for each sampling site ranged between 499.32 and 5945.46 mg/kg, where ST samples recorded the highest level of Pb. The minimum concentration of Pb found in SW samples was 499.32 mg/kg. All samples of weathering products in tailings and waste rock, soil, and sediments were considered to be polluted by Pb; this is probably related to the nature of the deposits, rich in lead, in the mining area. The maximum Cd content was found in SH samples, polluted by AMD heavily loaded with metals and with an average concentration of 95.50 mg/kg. The minimum average value of 19.47 mg/kg was recorded in SD samples, while in ST samples, the content did not exceed 20.23 mg/kg. This reflects very high contamination even for sediments. The average Fe concentrations detected in all samples were very high, with a maximum value of 330,824.83 mg/kg in SW samples. The Zn levels found in the different samples showed maximum average values of 3430.10 mg/kg at SH points. The minimum average concentration of Zn found in ST samples was 2072.16 mg/kg. Considerable Zn levels of 2836.80 mg/kg were found in SD samples; this is due to runoff waters that end up at the Guenitra dam. The maximum average concentration of Mn found in ST samples was 15,958.46 mg/kg; this content comes from tailings piles. The minimum level was 815.16 mg/kg at SH points. Average concentrations of Ni detected in SH samples, polluted by AMD, heavily loaded with metals, showed a maximum value of 239.91 mg/kg. The other samples had low Ni concentrations: 61.33 mg/kg for ST samples, 55.30 mg/kg for SD samples, and 18.63 mg/kg for SW samples. The Cr amount ranged from 28.97 mg/kg at SH points to 15.53 mg/kg in SD samples. Hg is a highly toxic metal generally present in small quantities. In fact, the levels found in all samples are considerable, with 75.95 mg/kg in ST samples and 4.22 mg/kg in SD samples. The Cu levels found in SD, ST, SH, and SW samples were 35.64, 85.52, 21.64, and 0.81 mg/kg, respectively.

The highest concentrations of Pb, Mn, Cu, and Hg metals were found in weathering products in ST samples. In addition, Zn, Cd, Ni, and Cr were found in SH samples affected by AMD, and Fe was found in SW samples. In this study, the total metal average concentrations in the four samples ST, SH, SW, and SD follow the order:

ST: Fe > Mn > Pb > Zn > Cu > Hg > Ni > Cd > Cr.

SH: Fe > Zn > Mn > Pb > Ni > Cd > Cr > Cu > Hg.

SW: Fe > Mn > Zn > Pb > Cd > Ni > Cr > Hg > Cu.

SD: Fe > Zn > Mn > Pb > Ni > Cu > Cd > Cr > Hg.

The most abundant metal in all samples was Fe, followed by Zn, Mn, and Pb. The least abundant was Cr and Cu.

The degree of pollution in the samples was assessed by comparing the concentration values obtained for the analyzed metals to Italian law standards. This law considers two levels of pollution: level A: upper limits for residential areas; level B: upper limits for industrial areas. All statistical boundaries of Pb, Cd, Zn, and Hg concentrations in ST samples exceeded level B. However, the Ni, Cr, and Cu values were lower than level A. For SH samples, Cd, Zn, and Hg exceeded level B. Pb and Ni exceeded level A, but Cr and Cu
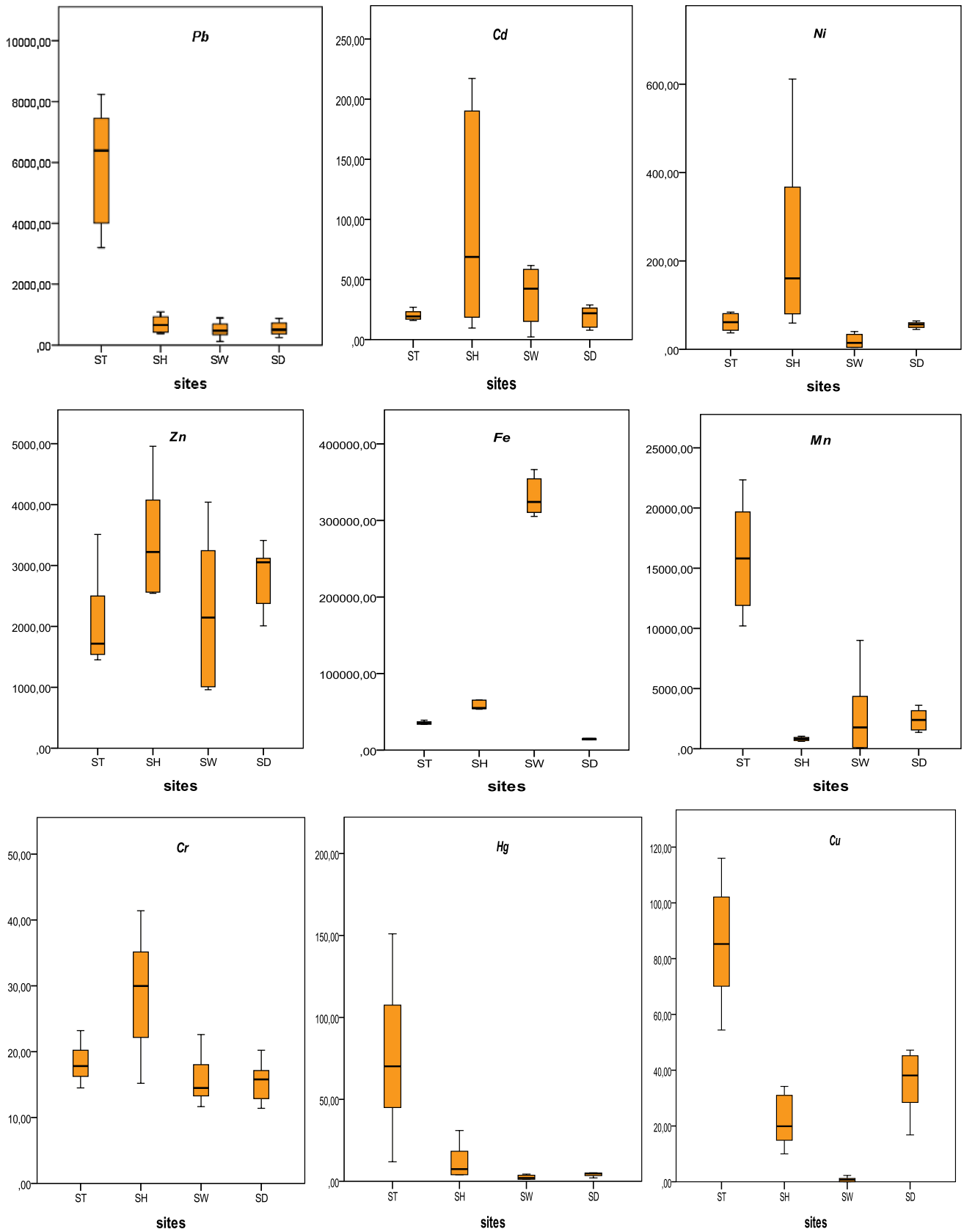
Fig. 2 Box plots of Fe, Cd, Zn, Cr, Pb, Cu, Mn, Ni, and Hg metal concentration (mg/kg) at the four sites ST, SH, SW, and SD ($N=6$)

Table 1 Descriptive statistics of selected chemical elements of mine wastes (ST and SW), soil (SH), and Guenitra dam sediments (SD)

Sites	Pb	Cd	Fe	Zn	Mn	Ni	Cr	Hg	Cu
Tailings (ST)									
pH 2.54									
Min	3200.33	15.90	33,700.00	1451.0	10,203.20	37.15	14.50	11.90	54.40
Max	8240.16	26.90	39,100.00	3510.0	22,340.60	84.20	23.20	151.0	116.0
Mean	5945.46	20.23	35,709.16	2072.16	15,958.46	61.33	18.30	75.95	85.52
Median	6386.42	19.26	35,326.50	1716.5	15,810.50	61.40	17.81	70.16	85.25
SD	1975.03	4.17	2074.566	798.19	4703.70	20.21	3.09	48.90	22.18
Soil (SH)									
pH 2.70									
Min	380.00	9.60	53,428.0	2543.20	611.60	59.4	15.2	3.98	10.0
Max	1083.20	217.2	65,425.00	4957.80	1037.00	611.6	41.40	30.98	34.20
Mean	684.52	95.5	58,036.16	3430.10	815.16	239.91	28.97	12.03	21.64
Median	650.83	68.75	54,978.00	3221.60	808.90	160.57	29.97	7.43	19.90
SD	286.32	89.58	5712.72	999.30	163.3	215.52	9.27	10.81	9.477
Waste rock (SW)									
pH 3.40									
Min	125.80	2.20	305,270.00	960.20	58.80	4.20	11.66	1.18	0.00
Max	889.00	61.60	366,467.00	4040.00	9001.80	40.20	22.60	4.40	2.26
Mean	499.32	37.00	330,824.83	2257.00	2839.83	18.63	15.76	2.41	0.81
Median	473.75	42.35	324,172.50	2144.70	1770.50	14.58	14.49	2.00	0.72
SD	267.02	24.85	25,106.11	1218.04	3519.14	15.48	3.95	1.34	0.85
Sediments (SD)									
pH 5.94									
Min	253.60	7.80	13,400.00	2009.00	1358.80	45.00	11.40	2.07	16.80
Max	871.20	28.80	15,062.00	3411.20	3609.00	64.20	20.22	5.20	47.20
Mean	536.98	19.47	14,426.50	2836.80	2411.26	55.30	15.53	4.22	35.64
Median	503.43	21.89	14,809.00	3052.80	2391.10	56.41	15.79	4.79	38.12
SD	228.34	8.63	781.66	529.25	907.94	7.19	3.18	1.22	11.42
Ref									
ILA	100	2	–	150	–	120	150	1	120
ILB	1000	5	–	1500	–	500	800	5	600

All values are in mg/kg, ($N=6$), IL: Italian laws for soils (level A* and B*). Level A: upper limits for residential areas. Level B: upper limits for industrial areas

SD standard deviation

were lower than level A. SW samples are classified into the same order as SD samples; the Ni, Cr, and Cu values were lower than level A. However, Pb and Hg exceeded level A, but only the highest statistical limits of Zn and Cd exceeded level B. These comparisons can be summarized in Table 2.

The chemical composition of major element oxides by XRF spectrometry for all samples is given in Table 3. There are significant variations in the concentrations of major oxides in all samples. XRF analysis reveals the presence of high portions of SiO_2 and Al_2O_3 in ST and SD samples and FeO (Tot) in the SW and SH samples, where the percentages of the three oxides are (43–65%), (15–19%), and (30–49%), respectively. Higher percentages of SiO_2 and Al_2O_3 demonstrated the dominance of aluminosilicate minerals in ST and SD samples. For FeO (Tot), the high percentages clearly showed a strong dominance of ferric oxyhydroxide in the

Table 2 Metal concentration comparison of ST, SW, SH, and SD by the two pollution level values (A and B) imparted by the Italian law

ST samples	SH samples	SW samples	SD samples
Pb, Cd, Zn, Hg > level B Ni, Cr, Cu < level A	Cd, Zn, Hg > level B Pb, Ni > level A Cr, Cu < level A	Cd, Zn > level B Pb, Hg > level A Cr, Cu, Ni < level A	Cd, Zn > level B Pb, Hg > level A Cr, Cu, Ni < level A

Table 3 XRF analysis of major element in ST, SH, SW, and SD samples (wt%)

Samples	ST_1	ST_2	SH_1	SH_2	SW_1	SW_2	SD_1	SD_2
FeO (tot)	8.368	7.868	30.367	30.043	49.170	49.098	5.300	5.219
CaO	0.578	0.641	0.266	0.254	0.200	0.158	1.030	1.029
SiO_2	43.898	47.827	3.634	3.102	2.002	1.207	65.001	65.180
MgO	0.622	1.087	0.186	0.236	0.122	0.138	1.186	1.397
Al_2O_3	16.963	19.362	1.259	1.431	0.192	0.142	15.741	15.813
MnO	0.014	0.027	0.001	0.001	0.001	0.001	0.080	0.071
ZnO	0.565	0.278	0.265	0.260	0.504	0.319	0.310	0.300
P_2O_5	0.103	0.036	4.348	4.232	0.001	0.001	0.048	0.053
Cr_2O_3	0.005	0.008	0.008	0.009	0.001	0.001	0.005	0.006
K_2O_3	2.553	3.708	3.348	3.005	0.098	0.074	2.541	2.607
Na_2O_3	1.345	0.888	1.608	0.710	0.190	0.101	5.522	5.589
SO_3	7.284	3.438	14.233	14.259	6.050	5.344	1.089	1.095
TiO2	0.797	0.822	0.056	0.053	0.022	0.023	1.018	1.020
LOI*	13.307	10.627	27.364	29.486	20.380	22.281	− 0.600	− 1.622

LOI loss on ignition at 1050 °C

SW and SH samples. However, other significant oxides are also observed in some samples, such as SO_3 (14%) and P_2O_5 (4%) in SH samples, which indicate a high sulphate and phosphate contents of this soil.

Statistical description of the metals concentrations

Table 4 shows a Pearson CM for analyzed metals. The parameters relationships support the results obtained from PCA and they also revealed a new metal association that had not been properly analyzed by PCA. A significant correlation has been observed in the samples. Pb significantly and positively correlates with Mn ($r=0.98$), Cu ($r=0.92$), and Hg ($r=0.99$). Cd also shows significant correlation with Cr ($r=0.93$), Ni ($r=0.91$), and Zn ($r=0.787$). Zn–Ni, Zn–Cr, and Ni–Cr metal pairs correlate significantly with respective correlation coefficient (r) values of 0.84, 0.75, and 0.98. Mn correlates with Hg ($r=0.97$) and Cu ($r=0.89$), A significant

correlation exists between Hg and Cu ($r=0.92$). However, no correlation was found for Fe with other metals.

Multivariate analysis of all samples was performed using HCA and PCA/FA techniques. Figure 3a, b shows a load graph of the principal components (PCs) and the dendrogram of metal elements obtained by HCA. PCA is a multivariate statistical technique that was performed to define the sources and groups of samples. In this PCA study, the calculation was limited to two factors; the total percentage of the variance expressed by these factors is about 70%. Factor F1 (42% of the total variance) is positively correlated with Pb, Mn, Hg, and Cu and negatively with Fe, Cd, Zn, Ni, and Cr (Table 5). It presents the first source of high concentration metals (tailing piles), in this case, and according to several studies (Ma et al. 2015; Kumar and Maiti 2015), this anthropogenic source is highly concentrated in metals that exceed largely geological background. This mining waste comes mainly from human activities during the exploitation and processing of minerals. Factor F2 (28% of the total variance)

Table 4 Correlation matrix of metals obtained using Pearson coefficients in all samples

	Pb	Cd	Fe	Zn	Mn	Ni	Cr	Hg	Cu
Pb	1.000								
Cd	− 0.399	1.000							
Fe	− 0.348	− 0.007	1.000						
Zn	− 0.604	0.787**	− 0.374	1.000					
Mn	0.988**	− 0.523	− 0.264	− 0.713	1.000				
Ni	− 0.189	0.914**	− 0.410	0.848**	− 0.337	1.000			
Cr	− 0.112	0.937**	− 0.301	0.753**	− 0.260	0.983**	1.000		
Hg	0.996**	− 0.322	− 0.391	− 0.534	0.970**	− 0.101	− 0.024	1.000	
Cu	0.921**	− 0.428	− 0.665	− 0.392	0.895**	− 0.098	− 0.091	0.925**	1.000

*Correlation is significant at the 0.05 level

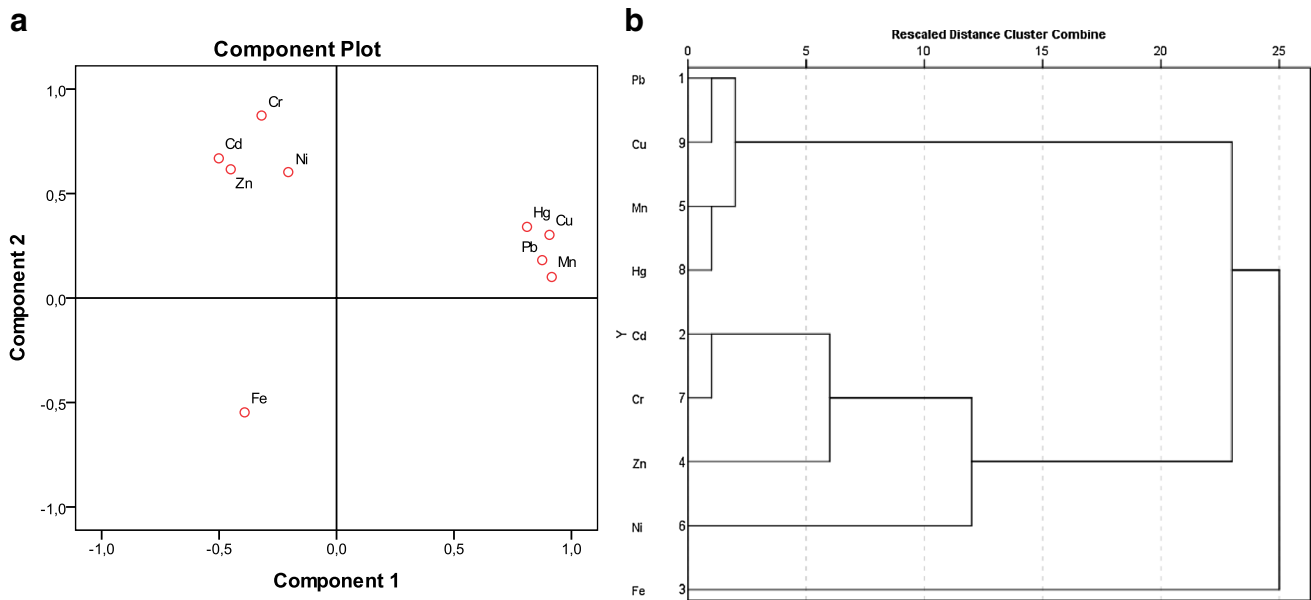**Correlation is significant at the 0.01 level

Fig. 3 Multivariate statistical analyses of metals: **a** principal component loading plot in PCA results and **b** dendrogram of the metal elements obtained by hierarchical cluster analysis

Table 5 Factor loadings of PCA analysis

Variable	F1	F2
Pb	0.876	0.181
Cd	− 0.501	0.668
Fe	− 0.391	− 0.547
Zn	− 0.450	0.616
Mn	0.916	0.101
Ni	− 0.206	0.603
Cr	− 0.319	0.873
Hg	0.811	0.341
Cu	0.907	0.302
Eigenvalues	3.837	2.502
% Variance explained	42.634	27.800
% Cumulative variance	42.634	70.434

is correlated positively with Cd, Zn, Ni, and Cr, and negatively with Fe (Table 5). This factor can be considered as a second source of high concentration metals, these metals come from soils highly polluted by AMD from old mining. This factor represents a mixed source of soil contamination by metals (lithogenic and anthropogenic). It should be noted that soil contamination by metals was also affected by the primary soil properties (Tian et al. 2016; Zhang et al. 2018).

On the other hand, HCA of all samples was performed using Ward's method with squared Euclidean distances as a measure of similarity. The dendrogram generated from HCA is illustrated in Fig. 3b. These metals could be classified into three distinct groups. C1 consisted of Pb, Mn, Hg, and

Cu, with anthropogenic origins mainly from tailings piles during mining activities. C2 including Cd, Zn, Ni, and Cr could be defined as a combination of natural and anthropogenic origins. This confirms the findings of PCA analysis. Fe clustered as C3; this group was not very clear in PCA/FA analysis and was different from other elements, which means that the source of Fe was not only from the parent materials, and Fe contents are essentially associated with the oxidation of pyrite (FeS_2) and the weathering of waste rock particles (lithogenic and anthropogenic).

In this area, generally, there were probably no significant natural sources, where mining waste from human activities was the main responsible for the high content of metals. The differences in factors are linked to the sedimentary environment and the chemical components (Lu et al. 2019).

Furthermore, Fig. 4a, b shows also the projection of individuals on the factorial plan F1–F2 and dendrogram of the study sites which revealed the existence of four different groups of samples with specific pollution profiles and localization:

- Group 1 contains ST1, ST2, ST3, ST4, ST5, and ST6 includes all samples collected at ST site which have similar characteristics;
- Group 2 consists of SW1, SW2, SW3, SW4, SW5, and SW6 samples, this group contains SW samples containing high concentrations of Fe;
- Group 3 is composed of SH1, SH2, SH3, SH4, SH5, and SH6; it indicates samples in SH site, with high concentrations of metals and high levels of pollution;
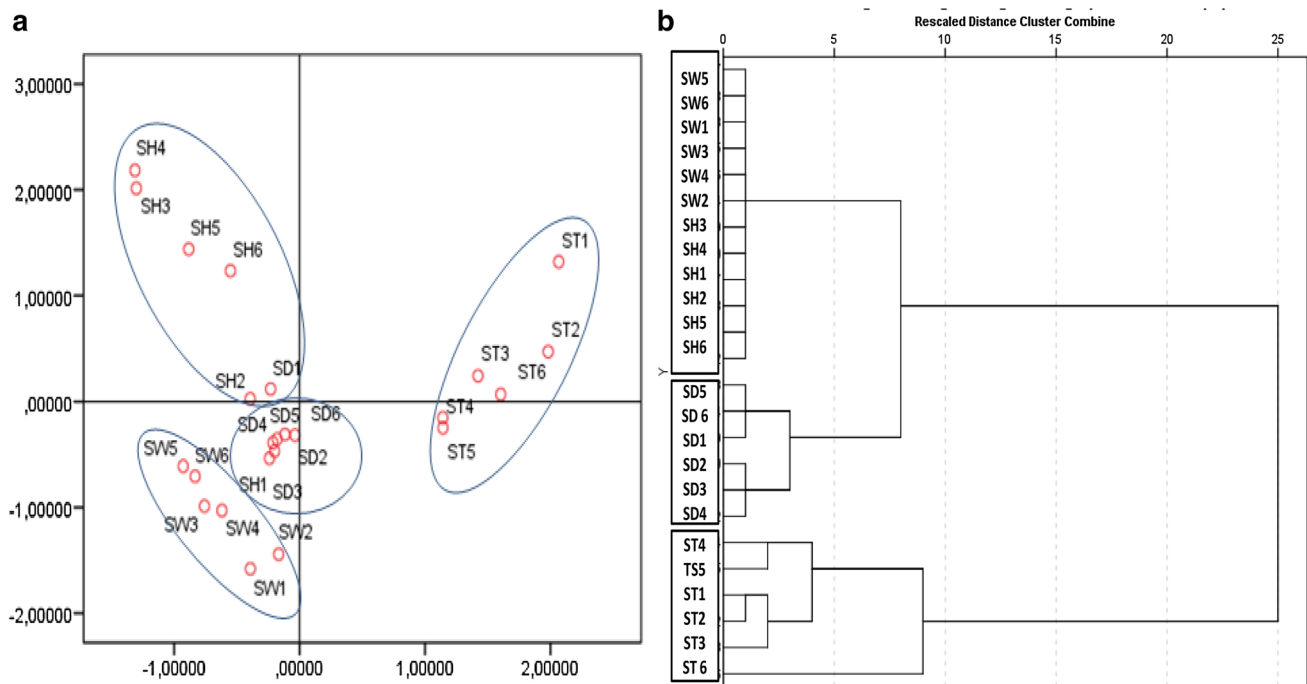
a

b

Fig. 4 Multivariate statistical analyses of the study sites: **a** principal component loading plot in PCA results and **b** dendrogram of the study sites obtained by hierarchical cluster analysis

- Group 4 includes SD1, SD2, SD3, SD4, SD5, and SD6, with moderate concentrations, which is a characteristic of the Guénitra dam sediment samples that are relatively characterized by a weak concentration of metals.

HAC analysis (Fig. 4b) gives us the same results as PCA analysis. Only groups 2 and 3 were regrouped in the same cluster due probably to the common source (lithogenic and anthropogenic) of metal pollution.

Mineralogical characterization

XRD mineralogical analysis

XRD analyses of ST, SH, SW, and SD samples were carried out to identify the mineral phases and crystallinity in each sample. Figure 5 shows X-ray mineralogy distinctly for all samples; and these latter contain several phases. The assessment of XRD mineralogical peaks for the presence of minerals in the samples was carried out with the help of the literature available (Lukasz et al. 2011; Saikia et al. 2015a, b, 2016), by comparison with inorganic compound powder diffraction file (PDF) database of the International Center for Diffraction Data (ICDD 2017). Significant proportions of muscovite ($KA_{12}(AlSi_3O_{10})$ $(OH, F)_2$) are present with moderate peak intensities in all samples, along with minor proportions of kaolinite ($Al_2Si_2O_5(OH)_4$) and lepidocrocite (γ-FeOOH) with low-peak intensities in ST and SD samples.

Ferrohexahydrite ($FeSO_4 \cdot 6H_2O$) and goethite (α-FeOOH) are the common minerals and the most prominent peak present in ST, SH, and SW samples. However, quartz (SiO_2) was the common mineral present in both ST and SD samples and the most prominent peak in the SD sample. The peaks present in the pattern of SH sample show clearly that jarosite (KFe_3 $(SO4)_2(OH)_6$) was the major component. Mineralogical analysis of the SW samples from waste rock showed the presence of ferrohexahydrite ($FeSO_4 \cdot 6H_2O$), goethite (α-FeOOH) and a significant proportion of amorphous material hematite (Fe_2O_3) with low crystallinity presented in XRD analysis by low peaks intensities. XRD analysis of all collected samples showed the presence of primary minerals such as quartz, muscovite, as well as secondary minerals such as iron oxyhydroxides (goethite), jarosite, and ferrohexahydrite. Silicate minerals found in this study belong to rocks of ore deposits and secondary minerals appear usually from existing primary minerals transformation, controlled by several parameters, such as short and long term variations in pH, aqueous speciation, bacterial activity, Eh, and mineral saturation (Marescotti et al. 2012; El Amari et al. 2014).

FTIR analysis

The identification of a mineral by infrared spectroscopy and the acknowledgment of its presence in mixtures are increasingly sure when its absorption bands are numerous and sharply characterized and if there appears a distinctive
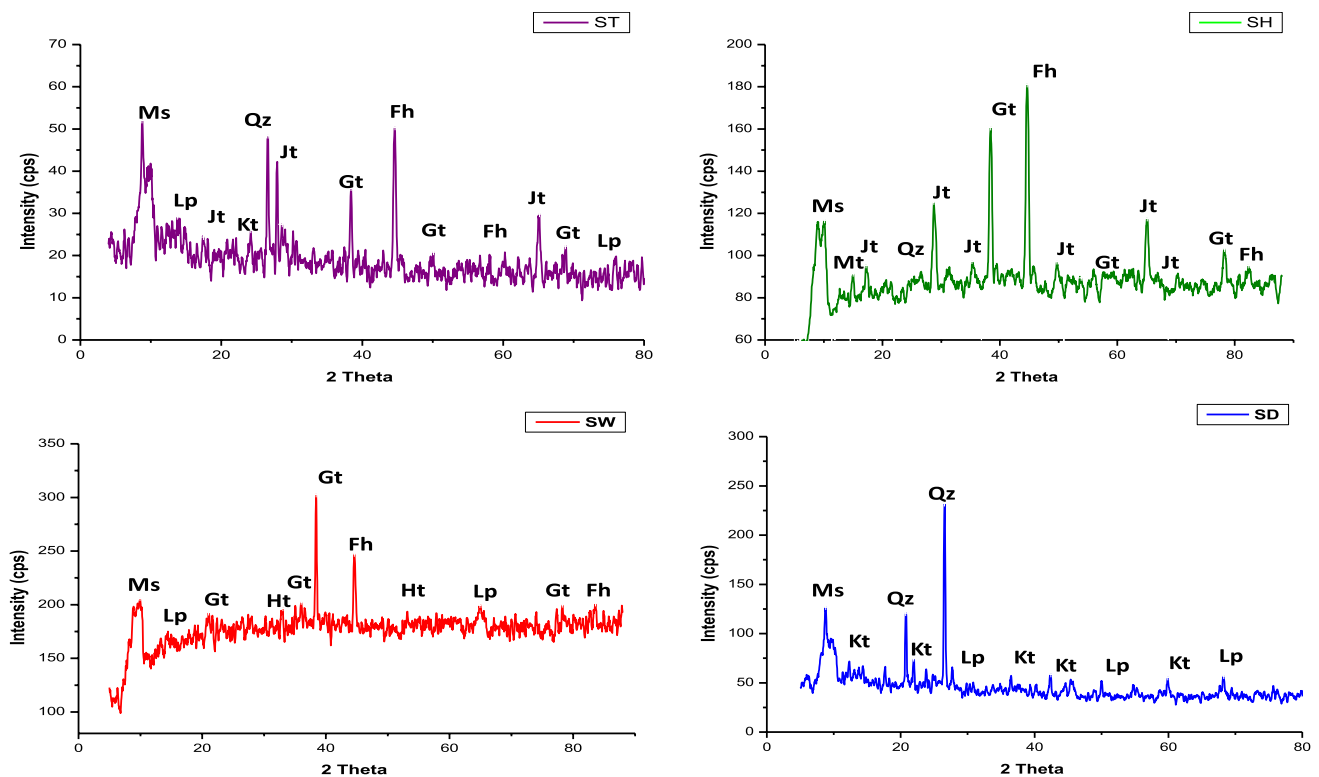
Fig. 5 XRD patterns of ST, SH, SW, and SD samples (Gt: Goethite, Fh: Ferrohexahydrite, Jt: Jarosite, Kt: Kaolinite, Lp: Lepidocrocite, Qz: Quartz, Ht: Hematite, Ms: Muscovite)

region of the spectrum. A sharp absorption band for the most part reflects a high level of crystallinity and regularity in the structure, so that the random isomorphic substitution, a characteristic common to silicates, tends to widen the absorption bands and reduce the details in the spectrum (Aroke et al. 2013). A comparison of FTIR spectra in the 400–4000 cm^{-1} region for all samples was carried out and the respective spectra are shown in Fig. 6. The interpretation of FTIR spectra is based on many studies and compared with the previous results of XRF and XRD techniques. The small peak at 3618–3619 cm^{-1} in ST and SD samples is assigned to the vibration of the Si–OH band found in the compounds containing Si silica (Van der Marel and Beutelspacher 1976). The presence of O–H-stretching bands for the three samples ST, SH, and SW may also be due to the presence of ferric oxyhydroxide and oxyhydroxysulfate, which may have contributed to the appearance of this band in the regions 3377 cm^{-1} in ST samples, 3372 cm^{-1} in SH samples, and a very broad band at 3151 cm^{-1} in SW samples. These results have already been confirmed by XRD. The same above-mentioned reason is behind the existence of the two peaks of less intensity at 882 and 591 cm^{-1} in SW samples, which corresponds to the vibrations of ferric oxyhydroxide (Bigham et al. 1990). All mineral samples ST, SH, SW, and SD show absorption bands close to 1632

and 1646 cm^{-1}, and are due to bending vibration of O–H bands of water, but the intensity of these bands in the spectra of all four samples is low. The broad and intense band appearing in the 1001–1019 cm^{-1} region has been assigned to the asymmetrical-stretching vibration of Si–O–Si in all ST, SH, SW, and SD samples (Smith 1999). The absorption bands for S–S and S–O in sulphates occur at 627 cm^{-1} for stretching vibration and 1082 cm^{-1} for bending vibration, respectively, in the SH sample (Baruah et al. 2003). It should be noted that ST and SD samples were very similar for all absorption bands with some differences in intensity. This result indicated that they have the same basic chemical structure and are characterized by the appearance of an intense band at 3377 cm^{-1} in the ST sample that may correspond to stretching vibrations of the O–H band of ferric oxyhydroxides. The spectra confirm the presence of bands particularly characterizing clay type. Most peaks in FTIR spectra between 4000 and 400 cm^{-1} can be attributed to clay minerals such as the quartz and kaolinite groups (Baruah and Khare 2007). In contrast, there is a series of bands between 911 and 520 cm^{-1}, which are detectable in the spectrum of $H_2Si_2O_5$ hydrated silica in ST and SD samples; this absorption is attributable to Si–O vibrations of quartz and mineral clays. A band bending occurring at 911 cm^{-1} in the spectrum of ST and SD samples was also noted, which implies the
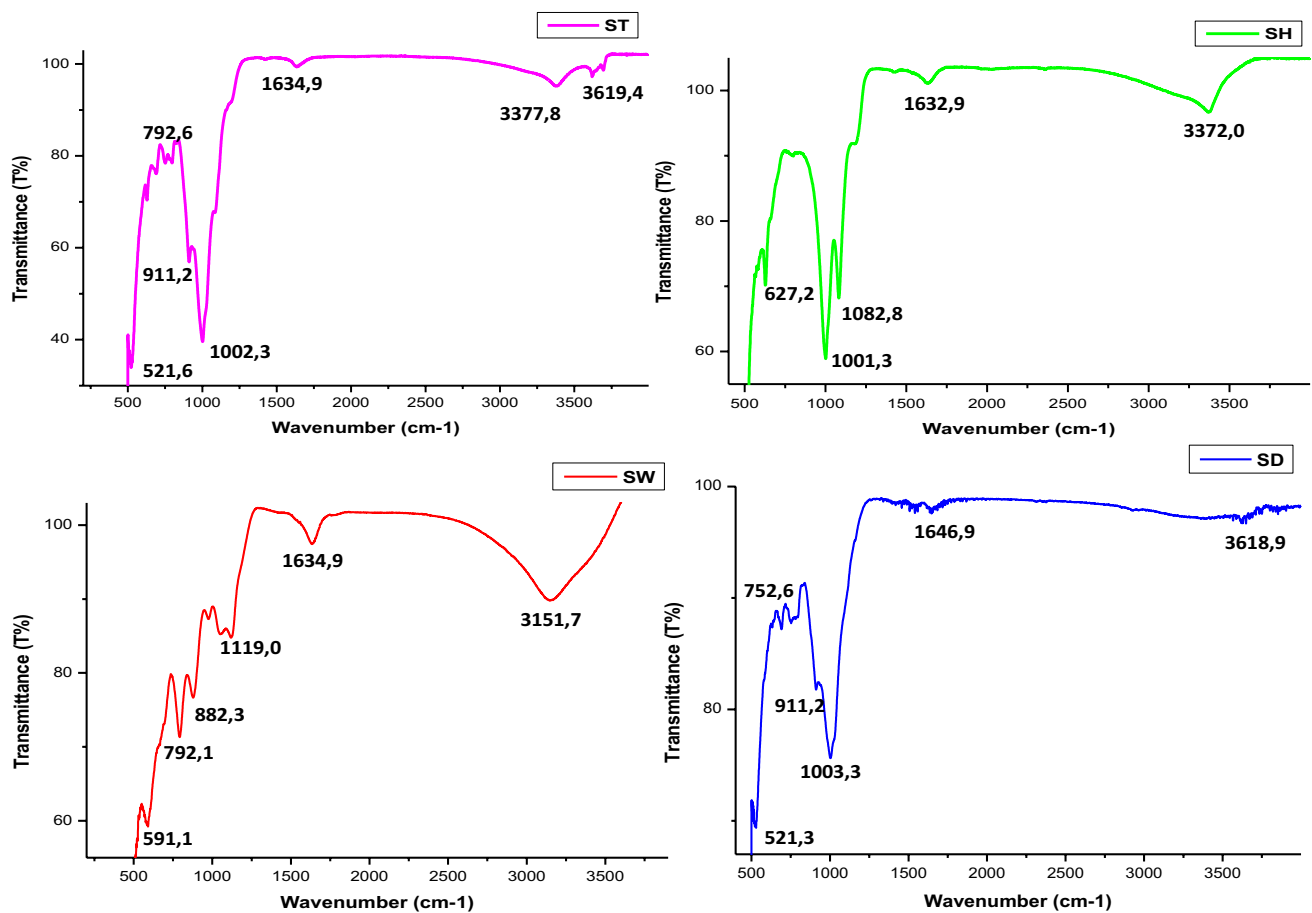
Fig. 6 Transmittance infrared spectra of ST, SH, SW, and SD samples

presence of Al–OH in these samples (Kalt and Wey 1968; Louhi et al. 2012).

Observation from SEM–EDX analysis

The SEM photomicrographs and EDX analyses of weathering products in mine wastes (tailings and waste rocks), soil affected by AMD, and Guenitra dam sediments are shown in (Fig. 7). SEM and EDX investigations for the present study have revealed many phases with different morphology and varying particle size. The obtained results from EDX analyses showed the heterogeneous composition of the four samples. The SEM results for some samples present complex aggregates and fibers, with more spheroidal and symmetrical forms, while the other samples indicated a more dense appearance reflecting its high percentage of amorphous phases. The interpretations of SEM results are based on certain studies of the mineralogy characterization and morphology of natural minerals (Saikia 2009; Saikia et al. 2015a, b; Oliveira et al. 2014; Pérez-Sirvent et al. 2016; Xie et al. 2018), for example, the study by Saikia et al. (2015a, b) shows that quartz is

euhedral and hexagonal in shape. EDX spectrum of ST samples indicates the presence of aluminium, silicon, and iron phases with significant quantity in addition to potassium, sulphate, sodium, magnesium, and titanium. SEM photographs of ST samples showed that some of the compositions suggest the presence of ferrohexahydrite and goethite minerals. The obtained results from EDX analyses of SH samples showed the same apparent composition in ST samples, with a remarkable difference in the amount of sulphate that is higher in SH samples; this latter also contains a high content of phosphorus and a significant amount of iron. SEM photographs of SH samples reveal the predominance of jarosite and ferrohexahydrite. EDX results of SW samples confirm the presence of iron with significant quantity, aluminium, silicon, and sulphate. SEM results of SW samples revealed the predominance of iron oxy-hydroxide, particularly goethite and hematite, which represent the amorphous character (Pérez-Sirvent et al. 2016). The SD samples also contain silicon and iron minerals with aluminium. In general, the representative SEM microphotographs of SD samples contain quartz and kaolinite.
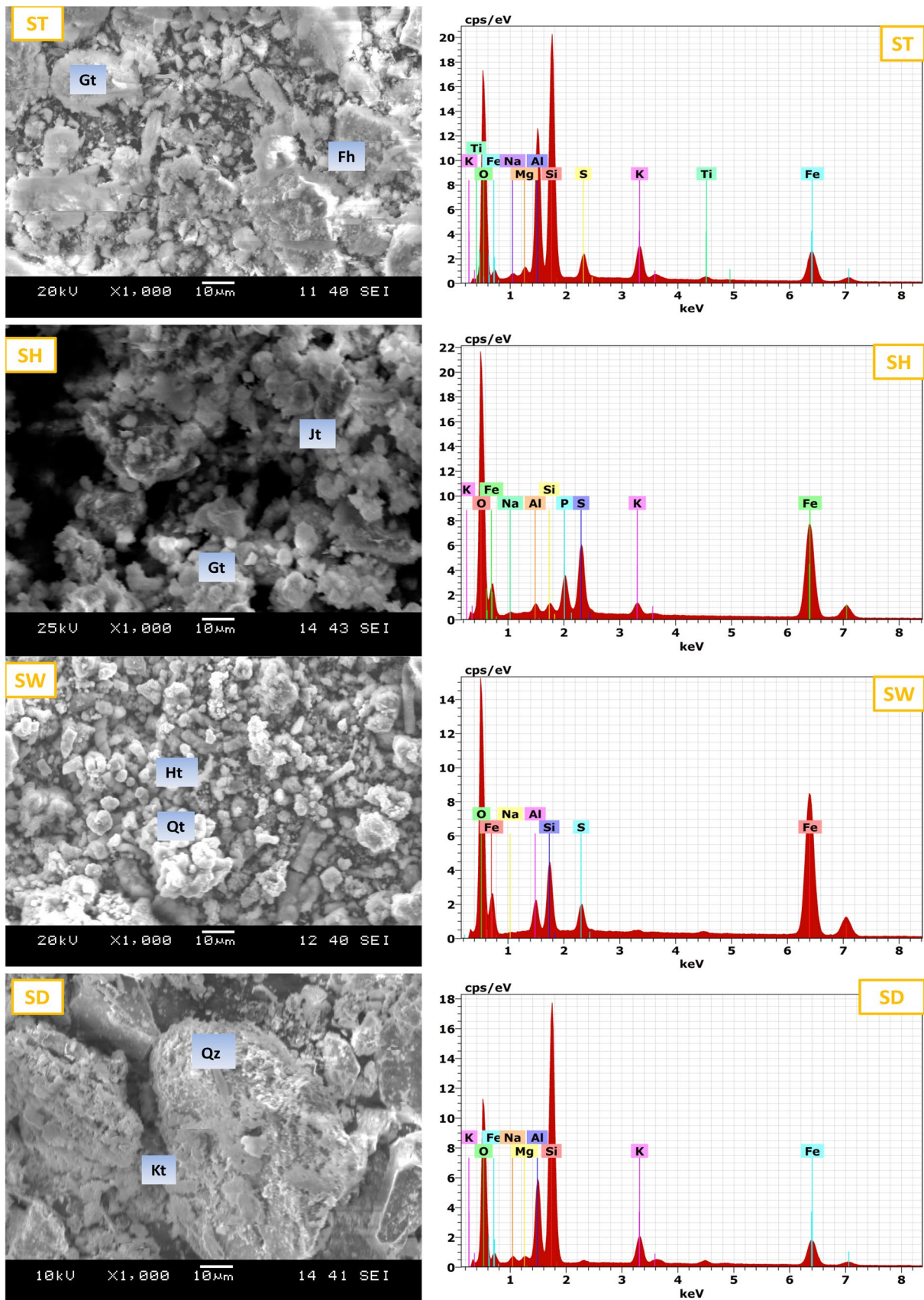
Fig. 7 SEM image and EDS spectra for ST, SH, SW, and SD samples

Conclusion

After more than 40 years from the closure the Sidi Kamber Pb/Zn mine in northeast Algeria, this latter remains a serious source of pollution by metals. In this study, three sources of pollution by metals have been identified: waste rock, tailing piles, and AMD of old mine water. Runoff from tailing piles, large expanses of waste rock rich in iron precipitate, and AMD often involve complex interactions between them and the surrounding environment, especially the closest soils to these sources and sediments of Guenitra dam downstream of the abandoned mine. To examine the environmental impact of the abandoned Sidi Kamber Pb/Zn mine, samples from weathering products in mine wastes, soil affected by AMD, and Guenitra dam sediments were collected and subjected to a detailed chemical analysis of metals and mineralogical characterization at each site. Distributions of metals in the three samples, weathering products in mine wastes (tailings and waste rock) and soil affected by AMD, showed serious contaminations with some metals such as Zn, Fe, Pb, Mn, Hg, and Cd due to the leaching of tailing and waste rock rich in iron precipitate and AMD of groundwater mine heavily polluted by sulphates and metals. On the other hand, Guenitra dam sediments are less contaminated with high values for certain metals such as Zn, Fe, and Cd. PCA/FA, as well as HCA classification showed that Cu, Mn, Hg, and Pb are derived from anthropogenic sources of tailings piles and that Ni, Zn, Cr, and Fe are most likely derived from lithogenic and anthropogenic sources.

According to the obtained mineralogical characterization results, weathering products in mine wastes, soil, and sediments were mainly composed of goethite, ferrohexahydrite, jarosite, hematite, and lepidocrocite. In addition, quartz, muscovite, and aluminium silicates such as kaolinite were also identified. The results confirm the need for using simultaneously chemical analysis and mineralogical characterization by multiple techniques to determine the potential risk and environmental impacts in these mining areas. Based on the obtained results, it is evident that the old abandoned Sidi Kamber mine exhibits a very serious environmental risk; therefore, actions to control the potential pollution and rehabilitation programs for these highly contaminated areas should be implemented. In addition, the remediation of contaminated soil by toxic metals is urgent to preserve the population health and the environmental restoration, through current in situ treatment technologies, such as the use of soil amendments by adsorption/precipitation, as well as phytoremediation, which is based on hyper-accumulative plants of metals.

References

Acero P, Ayora C, Torrento C, Nieto JM (2006) The behavior of trace elements during schwertmannite precipitation and subsequent transformation into goethite and jarosite. Geochim Cosmochim Acta 70:4130–4139

Aroke UO, Abdulkarim A, Ogubunka RO (2013) Fourier-transform infrared characterization of kaolin, granite, bentonite and barite. ATBU J Environ Technol 6:42–53

Baruah BP, Khare P (2007) Pyrolysis of high sulfur Indian coals. Energy Fuels 21:3346–3352

Baruah MK, Kotoky P, Borah GC (2003) Distribution and nature of organic/mineral bound elements in Assam coals, India. Fuel 82:1783–1791

Beddai OF (1976) Minéralisation de Sidi-Kamber. Rapport N°2, Laboratoire de Géologie appliquée, Université de Constantine

Bigham JM, Murad E (1997) Mineralogy of ochre deposits formed by the oxidation of iron sulfide. Adv Geoecol 30:193–226

Bigham JM, Schwertmann U, Carlson L, Murad E (1990) A poorly crystallized oxyhydroxysulfate of iron formed by bacterial oxidation of Fe(III) in acid mine waters. Geochim Cosmochimica Acta 54:2743–2758

Bigham JM, Schwertmann U, Traina SJ, Winland RL, Wolf M (1996) Schwertmannite and the chemical modeling of iron in acid sulfate waters. Geochim Cosmochim Acta 60:2111–2121

Bouhkalfa C (2007) Heavy metals in the water and sediments of Oued Es-Souk, Algeria, a river receiving acid effluents from an abandoned mine. Afr J Aquat Sci 32:245–249

Boukhalfa C, Chaguer M (2012) Characterisation of sediments polluted by acid mine drainage in the northeast of Algeria. Int J Sedim Res 27:402–407

Choo CO, Lee JK (2002) Mineralogical and geochemical controls on the formation of schwertmannite and goethite in the wetland at Dalseong tungsten mine, Korea. Geosci J 6:281–287

Dudka S, Adriano DC (1997) Environmental impacts of metal ore mining and processing: a review. J Environ Qual 26:590–602

El Amari K, Valera P, Hibti M, Pretti S, Marcello A, Essarraj S (2014) Impact of mine tailings on surrounding soils and ground water: case of Kettara old mine, Morocco. J Afr Earth Sci 100:437–449

Favas PJC, Sarkar SK, Rakshit D, Venkatachalam P, Prasad MNV (2016) Acid mine drainages from abandoned mines: hydrochemistry, environmental impact, resource recovery, and prevention of pollution. Environ Mater Waste 413–462

Gherib A, Djebaili H, Bouchaala L, Charchar N, Aissaoui A, Lehout A (2017) Physiological and biochemical markers in the process of resistance and/or tolerance of heavy metals in the abandoned mining area of Sidi Kamber, Skikda, Algeria. Int J Environ Stud 74:275–289

Hochella MF, Moore JN, Putnis CV, Putnis A (2005) Direct observation of heavy metal–mineral association from the Clark Fork River Superfund Complex: implications for metal transport and bioavailability. Geochim Cosmochim Acta 69:1651–1663

Iakovleva E, Mäkilä E, Salonen J, Sitarz M, Wang S, Sillanpää M (2015) Acid mine drainage (AMD) treatment: neutralization and toxic elements removal with unmodified and modified limestone. Ecol Eng 81:30–40

ICDD (2017) International center for diffraction data. http://www.icdd.com/. Accessed 27 Dec 2017

Jonsson J, Jonsson J, Lovgren L (2006) Precipitation of secondary Fe(III) minerals from acid mine drainage. Appl Geochem 21:437–445

Kalt A, Wey R (1968) Composés interfoliaires d'une silice hydratée cristallisée. Bulletin du Groupe français des Argiles 20:205–214

Kim JJ, Kim SJ, Tazaki K (2002) Mineralogical characterization of microbial ferrihydrite and schwertmannite, and no-biogenic Al-sulfate precipitates from acid mine drainage in the Donghae mine area, Korea. Environ Geol 42:19–31

Kumar A, Maiti SK (2015) Assessment of potentially toxic heavy metal contamination in agricultural fields, sediment, and water from an abandoned chromite-asbestos mine waste of Roro hill, Chaibasa, India. Environ Earth Sci 74:2617–2633

Laurel AS, David BS, Emily RE, Daniel JB, James PS (2014) Sources and fates of heavy metals in a mining-impacted stream: temporal variability and the role of iron oxides. J Sci Total Environ 490:456–466

Louhi A, Hammadi A, Achouri M (2012) Determination of some heavy metal pollutants in sediments of the Seybouse River in Annaba, Algeria. Air Soil Water Res 5:91–101

Lu J, Lu H, Lei K, Wang W, Guan Y (2019) Trace metal element pollution of soil and water resources caused by small-scale metallic ore mining activities: a case study from a sphalerite mine in North China. Environ Sci Pollut Res 26:24630–24644

Lukasz U, Stefan S, Michal S, Branimir S (2011) Clay-mineral formation in soils developed in the weathering zone of pyrite-bearing schists: a case study from the abandoned pyrite mine in wies´ciszowice, lower silesia, SW poland. J Clays Clay Min 59:581–594

Ma L, Sun J, Yang Z, Wang L (2015) Heavy metal contamination of agricultural soils affected by mining activities around the Ganxi River in Chenzhou, Southern China. Environ Monit Assess 187:731

Marescotti P, Carbone C, Comodi P, Frondini F, Lucchetti G (2012) Mineralogical and chemical evolution of ochreous precipitates from the Libiola Fe–Cu-sulfide mine (Eastern Liguria, Italy). Appl Geochem 27:77–589

Medjram S, Malika K (2014) Study and evaluation of risk related to waters contamination of dam of Guenitra, by heavy metals, from mine of Sidi Kamber. J Selcuk Univ Nat Appl Sci, pp 268–274

Navarro MC, Perez-Sirvent C, Martinez-Sanchez MJ, Vidal J, Tovar PJ, Bech J (2008) Abandoned mine sites as a source of contamination by heavy metals: a case study in a semi-arid zone. J Geoche Explor 96:183–193

NF EN 13346 (2000) Caractérisation des boues—Détermination des éléments traces et du phosphore- Méthodes d'extraction à l'eau régale

Oliveira MLS, Marostega F, Taffarel SR, Saikia BK, Waanders FB, Daboit K, Baruah BP, Silva LFO (2014) Nano-mineralogical investigation of coal and fly ashes from coal-based captive power plant (India): an introduction of occupational health hazards. Sci Total Environ 468–469:1128–1137

Oumedjbeur A (1986) Evaluation de la qualité physico-chimique des eaux du bassin versant du barrage de Guénitra (wilaya de Skikda). Thèse de Docteur de 3éme cycle, Université de Savoie

Pérez-Sirvent C, Hernández-Pérez C, Martínez-Sánchez MJ, García-Lorenzo ML, Bech J (2016) Geochemical characterisation of surface waters, topsoils and efflorescences in a historic metal-mining area in Spain. J Soil Sedim 16(4):1238–1252

Rashed MN (2010) Monitoring of contaminated toxic and heavy metals, from mine tailings through age accumulation, in soil and some wild plants at Southeast Egypt. J Hazard Mater 178:739–746

Rios CA, Williams CD, Roberts CL (2008) Removal of heavy metals from acid mine drainage (AMD) using coal fly ash, natural clinker and synthetic zeolites. J Hazard Mater 156:23–35

Rose S, Elliott WC (2000) The effects of pH regulation upon the release of sulfate from ferric precipitates formed in acid mine drainage. Appl Geochem 15:27–34

Rowe RK, Hosney MS (2013) Laboratory investigation of GCL performance for covering arsenic contaminated mine wastes. Geotext Geomembr 39:63–77

Saikia BK (2009) Scanning electron microscopy of Assam Coals, India. J Geol Soc India 74:749–752

Saikia BK, Wang P, Saikia A, Gupta UN, Song H, Liu JW (2015a) Mineralogical and elemental composition of some high sulfur Indian tertiary coals: statistical analysis of the oxides and elements. Energ Fuel 29:1407–1420

Saikia BK, Arpita S, Sahu OMP, Bimala PB (2015b) Study on physico-chemical properties, mineral matters and leaching characteristics of some indian coals and fly ash. J Geol Soc India 86:275–282

Saikia BK, Banashree M, Upendra NG, Sahu OMP, Saikia P, Bimala PB (2016) Mineralogical composition and ash geochemistry of raw and beneficiated high sulfur coals. J Geol Soc India 88:339–349

Silva LFO, Ortiz Fdez-, de Vallejuelo S, Martinez-Arkarazo I, Castro K, Oliveira MLS, Sampaio CH, de Brum Irineu AS, de Leão Felipe B, Taffarel SR, Madariaga JM (2013) Study of environmental pollution and mineralogical characterization of sediment rivers from Brazilian coal mining acid drainage. Sci Total Environ 447:169–178

Singh AN, Zeng DH, Chen FS (2015) Heavy metal concentrations in redeveloping soil of mine spoil under plantations of certain native woody species in dry tropical environment, India. J Environ Sci 17:168–174

Smith B (1999) Infrared spectral intrepretation a systematic approach. CRC Press, London

Tertian R, Claisse F (1982) Principles of quantitative X-ray fluorescence analysis. Heyden

Tian K, Hu W, Xing Z, Huang B, Jia M, Wan M (2016) Determination and evaluation of heavy metals in soils under two different greenhouse vegetable production systems in eastern China. Chemosphere 165:555–563

Tonkin JW, Balistrieri LS, Murray JW (2002) Modeling metal removal onto natural particles formed during mixing of acid rock drainage with ambient surface water. Environ Sci Technol 36:484–492

Van der Marel HW, Beutelspacher H (1976) Atlas of infrared spectroscopy of clay minerals and their admixtures. Elsevier Publishing Company, Amsterdam

Xie Y, Lu G, Yang C, Qu L, Chen M, Guo C, Dang Z (2018) Mineralogical characteristics of sediments and heavy metal mobilization along a river watershed affected by acid mine drainage. PLoS ONE 13:1–17

Zanuzzi A, Arocena JM, Mourik V, Faz Cano JMA (2009) Amendments with organic and industrial wastes stimulate soil formation in mine tailings as revealed by micromorphology. Geoderma 154:69–75

Zhang X, Tian Y, Shen M, Zeng G (2018) Heavy metals in soils and sediments from Dongting Lake in China: occurrence, sources, and spatial distribution by multivariate statistical analysis. Environ Sci Pollut Res 25(14):13687–13696